ChemComm

HIGHLIGHT

View Article Online
View Journal | View Issue

Cite this: *Chem. Commun.*, 2025, **61**, 10210

Electrochemical hydrogen pumps: a researcher's guide and review

Rory Bagacki, *[af] Maximilian Reinhardt,[a] Rutger Schlatmann, [be] Sonya Calnan, [bc] Roel van de Krol *[adf] and Michelle P. Browne *[a]

Received 31st March 2025,
Accepted 12th June 2025

DOI: 10.1039/d5cc01815c

rsc.li/chemcomm

Hydrogen is considered an attractive energy vector and an indispensable base chemical for a wide variety of chemical products. As more hydrogen is produced *via* electrolysis, finding ways to store the H_2 will become increasingly important due to the low volumetric energy density at ambient pressure. While high pressure storage is favoured for many applications, compressing hydrogen poses distinct challenges due to its low density and high diffusivity. Electrochemical hydrogen pumps (EHP) present a solution to this challenge by efficiently compressing hydrogen. Hydrogen compression is more efficient using electrochemical hydrogen pumps than conventional mechanical compressors because they operate through isothermal rather than adiabatic compression. Additionally, they can be used to separate hydrogen from gas mixtures, for example from natural gas pipelines supplemented with hydrogen, creating the possibility of integrating them with existing energy transport infrastructure. This paper summarizes recent progress in electrochemical hydrogen pump research and presents a case study on an EHP test cell, test rig and a measurement guide to advance research in this field. Although electrochemical hydrogen pumps offer many advantages, shortcomings remain, including the lack of standardized measurement conditions and procedures, as well as a limited understanding of degradation mechanisms. This review aims to provide insights into these issues and discuss future directions for electrochemical hydrogen pump research.

[a] *Helmholtz Young Investigator Group Electrocatalysis: Synthesis to Devices, Helmholtz-Zentrum Berlin für Materialien und Energie, 12489 Berlin, Germany. E-mail: rory.bagacki@helmholtz-berlin.de, michelle.browne@helmholtz-berlin.de*
[b] *Institut Kompetenz-Zentrum Photovoltaik Berlin (PVcomB), Helmholtz-Zentrum Berlin für Materialien und Energie, 12489 Berlin, Germany*
[c] *Wolfson School of Mechanical, Electrical and Manufacturing Engineering, Loughborough University, LE11 3TU Loughborough, UK*
[d] *Institute for Solar Fuels, Helmholtz-Zentrum Berlin für Materialien und Energie, 14109 Berlin, Germany*
[e] *Hochschule für Technik und Wirtschaft Berlin, 12459 Berlin, Germany*
[f] *Technische Universität Berlin, Institute of Chemistry, 10623 Berlin, Germany*

Rory Bagacki

Rory Bagacki holds an MASc in Mechanical Engineering from Queen's University and is currently a doctoral researcher at the Helmholtz-Zentrum Berlin in Michelle Browne's Electrocatalysis: Synthesis to Devices group, pursuing a doctorate at TU Berlin. His research interests include the development of electrocatalyst materials, electrolysis and hydrogen compression using electrochemical hydrogen pumps.

Maximilian Reinhardt

Maximilian Reinhardt holds an MSc in Physical Engineering from TU Berlin. He joined Sonya Calnan's group at HZB in 2022 as an engineer specializing in electrolysis and hydrogen compression. Since 2024, he has been continuing this work in Michelle Browne's group.

1. Introduction

Hydrogen is an essential reactant in various manufacturing processes. For example, hydrogen is utilized in the manufacturing of steel and in the Haber Bosch processes to make ammonia.[1] In order to decarbonize these hard to abate manufacturing sectors, the grey/blue H_2 currently used in these processes, made by reforming natural gas, is targeted to be replaced by green hydrogen. Furthermore, green hydrogen has been pinpointed as a key current and future energy carrier by the European Union (EU) to help reduce the amount of fossil fuel-based resources utilised to produce electricity for transport, building infrastructure and manufacturing processes.[2]

Green H_2 is produced by water electrolysis where water (acid or alkaline) is split into H_2 on the cathode and O_2 on the anode. This process is powered by a renewable energy technology such as photovoltaics or wind turbines and thus is an environmentally friendly route to make H_2. On the other hand, the synthesis of grey H_2 by steam methane reforming (SMR) utilizes fossil fuels and is a multi-step process. To produce H_2 by SMR, first syngas is formed which contains H_2, CO and small quantities of CO_2.[3] This is followed by the water–gas shift reaction, in which CO reacts with water to produce CO_2 and an additional hydrogen molecule. Then the H_2 is purified and separated by a variety of techniques, including pressure or temperature swing adsorption and cooling steps. However,

Rutger Schlatmann

Rutger Schlatmann heads the Solar Energy Division at Helmholtz-Zentrum Berlin and is the founding director of its technology transfer institute PVcomB. He is full professor for solar photovoltaics technology at the Hochschule fuer Technik und Wirtschaft Berlin. He worked as staff scientist at Akzo Nobel and R&D manager for solar cell company Helianthos (now HyET Solar). Since 2022, he is the elected Chairman of the European Technology and Innovation Platform Photovoltaics, an advisory committee to the European Commission, of which he has been a member since 2014. His research interests range from solar cells and modules to production technologies and outdoor systems, as well the application of thin film and nanostructured systems in catalytic applications for renewable chemicals and fuels.

Sonya Calnan

Sonya Calnan joined Loughborough University, UK in July 2024 as a full professor of Energy Engineering in the Wolfson School of Mechanical, Electrical and Manufacturing Engineering. Prior to that, she led the Photovoltaics to Fuels Technology research group at the Helmholtz-Zentrum Berlin, Germany. Her research interests include chemical reactor and process development for energy and fuels conversion using hydrogen and its derivatives.

Roel Van de Krol

Roel van de Krol is head of the Institute for Solar Fuels at the Helmholtz-Zentrum Berlin (HZB) and full professor at the Chemistry Department of TU Berlin since 2012. His group focuses on the development of materials and devices for the photoelectrochemical conversion of sunlight into fuels and value-added chemicals. This includes the development of deposition processes for thin film photoelectrodes and catalysts, and scale-up of solar fuel devices to the ~100 cm^2 scale. The group specializes in metal oxide absorbers and employs a range of surface science and ultra-fast spectroscopy techniques to understand their properties and identify performance bottlenecks.

Michelle P. Browne

Dr Michelle Browne is a Helmholtz Young Investigator Group Leader at Helmholtz-Zentrum Berlin (Germany) since July 2022. Her group is developing and understanding new materials, including MXenes, for the generation, utilization and transportation of green hydrogen. To date, Michelle has received numerous awards for her research including the 2025 Scholarship Program of the Daimler and Benz Foundation for the Promotion of Postdocs & Junior Professors and The Curious Minds Research Award 2023.

these syngas separation techniques have several key disadvantages associated with them which include not being able to be utilized continuously in the case of the adsorption-based separation methods.[3]

Regardless of the method by which H_2 is produced, one important factor that must be considered to reduce the cost of H_2 - yet remains unaccounted for in current market prices - is its transportation to end-use locations. Hydrogen can be transported as compressed gas, liquified H_2, liquid organic hydrogen carriers, or ammonia. Various transportation methods exist, including trucks, ships/barges, and pipelines with costs differing significantly, with pipelines being the more economic option.[4,5] Current gas pipeline infrastructure can be utilised now to transport blended H_2 with the goal of having dedicated H_2 pipelines in Europe by 2040.[6] Recently, Gascade Gastransport GmbH have started to already repurpose German gas pipelines and transport H_2 from the north of Germany, where the H_2 is produced off-shore, to the south of the country.[7] The need for H_2-only pipelines is essential for the transportation of highly concentrated H_2 because H_2 can damage the steel used to make conventional gas pipelines through hydrogen embrittlement.

For the transportation of blended H_2 in current gas pipelines, the H_2 must be de-blended from the natural gas, purified, and then compressed at the end-use location before being fed into downstream processes. The de-blending and purification must be economically viable to not increase the overall cost of the H_2 being transported. Currently, pressure swing adsorption (PSA) is one route used in industry to purify H_2. However, as reported by Jackson and co-workers, PSA would cost about one-third of the price of the transported H_2.[6] Hence, other less expensive ways of purifying H_2 must be taken into consideration. Another process which is essential for H_2 is its storage. Currently, mechanical pumps are utilised to compress H_2 at the point of use however, mechanical pumps can result in the significant loss of H_2 and thus, reduce the overall efficiency of H_2 compression.[8]

One electrochemical-based technology that is growing in interest to de-blend, purify and/or compress H_2 are electrochemical hydrogen pumps (EHP). EHP technology offers a one-stop solution for the deblending, purification, and compression of H_2 at the end-use location. EHPs were first developed by Electric Motors in the 1960s and mostly utilize perfluorosulfonic acid (PFSA), *e.g.* Nafion™, based membranes developed by Dupont.[9] The PFSA membrane is a proton conductor hence, other ions will not pass through the membrane, and the protons will be selectively separated from mixed blends. In recent years, research into developing other membranes for EHP has been ongoing as the Nafion™ membrane is not stable over approximately 80 °C. Moreover, the Pt catalysts used on the cathode and anode adsorb the CO from the syngas, which ultimately de-actives the active catalyst and decreases the efficiency of the EHP.

Though green hydrogen is a promising alternative to fossil fuel derived hydrogen for decarbonizing industrial, chemical and transport sectors, its adoption requires cost effective methods for deblending, purification and compression. Electrochemical hydrogen pumps offer a solution to these challenges, though limitations in membrane and catalyst stability and tolerance to impurities must be addressed for large-scale deployment of the technology.

1.1. Fundamental electrochemistry

In an EHP, the hydrogen oxidation reaction (HOR) occurs on the anode while the hydrogen evolution reaction (HER) proceeds on the cathode. The EHP process is initiated by H_2 gas, along with the other gases in the pipeline, flowing to the anode and being oxidized into protons and electrons. The protons will travel through the membrane and the electrons will travel through the external circuit. At the cathode, through the HER, the protons will be reduced and molecular H_2 will be formed. As both the HER and HOR in an EHP occur under PEM-compatible (acidic) conditions, the state-of-the-art catalyst used for both reactions is platinum.

In acidic conditions, the HOR proceeds as

$$H_2^{LP} \rightarrow 2H^+ + 2e^-, \quad E^0 = 0.0\ \text{V } \textit{vs.}\ \text{SHE} \tag{1}$$

While the HER follows

$$2H^+ + 2e^- \Leftrightarrow H_2^{HP}, \quad E^0 = 0.0\ \text{V } \textit{vs.}\ \text{SHE} \tag{2}$$

Leading to the overall electrochemical reaction of an EHP is as follows

$$H_2^{LP} \Leftrightarrow H_2^{HP} \tag{3}$$

HOR/HER on Pt may proceed *via* Heyrovsky–Volmer mechanism and the rate limiting step is believed to be either the Volmer or Heyrovsky step, although other mechanisms seem possible.[10] This uncertainty is caused by the difficulty in accurately pinpointing the rate limiting step, by experiment, because of the inherently high speed of these reactions.[11] Nevertheless, the symmetry of HOR and HER on Pt suggest that they have the same reaction mechanisms and are thus fully reversible.[11] The equations for the different steps are

$$\text{Tafel: } H_2 + 2^* \Leftrightarrow H_{ads} + H_{ads} \tag{4}$$

$$\text{Heyrovsky: } H_2 + {}^* + H_2O \Leftrightarrow H_{ads} + H_3O^+ + e^- \tag{5}$$

$$\text{Volmer: } H_{ads} + H_2O \Leftrightarrow {}^* + H_3O^+ + e^- \tag{6}$$

The ideal EHP can be considered to operate under the following assumptions

- Hydrogen behaves as an ideal gas
- Isothermal compression such that the temperature T [K] of the hydrogen gas does not change after compression and $\Delta T = 0$
- The EHP is a thermodynamically open system through which hydrogen flows, see Fig. 1. Additionally, the volume V [cm^3] of the EHP remains constant with time, *i.e.*, $\Delta V = 0$

The EHP operates when a high enough voltage, E_{EHP}, is applied to its terminals driving the transfer of protons across the PEM, leading to a net current, I_{EHP}. The total charge transferred per mole of hydrogen oxidized during operation of the EHP is given by

$$Q = zeN_{Avg} \tag{7}$$

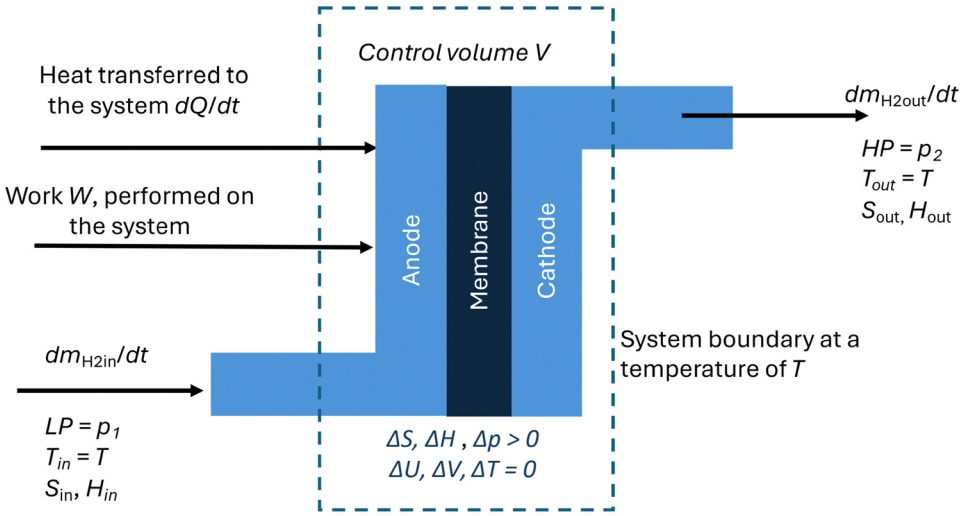

Fig. 1 Representation of an electrochemical pump as an open thermodynamic system operating at steady state under isothermal conditions. The changes in volume, ΔV, temperature, ΔT, and internal energy, ΔU, are all zero, whereas the changes in entropy, ΔS, enthalpy, ΔH, and pressure, Δp, are non-zero. The work W performed on the system compresses hydrogen from low pressure (LP), p_1 to a high-pressure (HP), p_2 and heats the system by dQ.

where z is the number of electrons transferred per mole of hydrogen, where $z = 2$, e is the electronic charge = 1.602×10^{-19} C and N_{Avg} is Avogadro's number, which is the number of molecules per mole of a gas (6.022×10^{23} molecules mol^{-1}).

Note that eN_{Avg} = 96 485 C mol^{-1}, also known as Faraday's constant, F. Thus, the maximum work available to compress n moles of gas within a time, t (s), is provided by the electrical power input, W_{el}, given as

$$W_{el} = E_{EHP}\, I_{EHP} = 2nFE_{EHP}/t \quad (8)$$

From thermodynamics, the reaction's Gibb's free energy G_r is defined as the energy used to change the system state from equilibrium and is given by

$$G_r = H_r - TS_r \quad (9)$$

Then the Gibbs energy of formation or dissociation of hydrogen under isothermal conditions is

$$\Delta G_r = \Delta H_r - T\Delta S_r \quad (10)$$

where the enthalpy of reaction H_r is the chemical energy involved in $2H^+/H_2$ reactions and S_r is the entropy that describes the irreversible loss of energy during the reaction. Under reversible conditions, all the electrical energy supplied to the EHP is used for compression, so that the isothermal compression work, $W_{iso,rev}$, is defined by

$$W_{el,rev} = W_{iso,rev} \quad (11)$$

This reversible isothermal compression work is also equivalent to the Gibbs energy of formation (and dissociation) of hydrogen. In this situation, the second term of the right-hand side of eqn (10) is zero and the EHP voltage is referred to as the reversible voltage E_{rev}, then

$$\Delta G_{rev} = -2F\, E_{rev} \quad (12)$$

Re-writing, the reversible voltage is

$$E_{rev} = \Delta G_{r,rev}/2F \quad (13)$$

Also, the thermodynamics definition of mechanical work done to compress the hydrogen, ΔU_{mec} is

$$\Delta U_{mec} = \Delta(pV) = V\Delta p \quad (14)$$

For isothermal conditions,

$$\Delta G_r = V\Delta p \quad (15)$$

From the ideal gas law,

$$\Delta G_r = nRT\Delta p \quad (16)$$

For an infinitesimal change in pressure, the temperature can be considered constant, such that the changes can be expressed by the respective differentials ($\Delta \rightarrow d$) giving

$$dG_r = dp\ (nRT/p) \quad (17)$$

Integrating G_r and p over the span of the initial and final states. denoted "i" and "f", gives

$$(G_{r,f} - G_{r,i}) = (RT/n)\ (\ln(p_f) - \ln(p_i)) \quad (18)$$

Rearranging and assuming compression from standard conditions, *i.e.* $E_i = E^0$, $p_i = p^0$, $n = 1$, and Gibbs energy at standard conditions G_r^0

$$G_{r,f} = G_r^0 + RT/n \ln(p_f/p^0) \quad (19)$$

Re-writing eqn (20) using the relation in eqn (13), e and re-arranging yields the reversible cell voltage E_{rev} [V]

$$E_{rev} = E_r^0 + (RT/2F)\ln[(p_{HP}/p^0)/(p_{LP}/p^0)] \quad (20)$$

But for $2H^+/H_2$, $E^0 = 0$, thus

$$E_{rev} = (RT/2F)\ln[(p_{HP}/p^0)/(p_{LP}/p^0)] \quad (21)$$

The thermoneutral voltage E_{tn} is defined as the potential at which the EHP can be operated without any heat loss or gain

from the environment. It can be determined using a procedure reported by Godshall under consideration of isothermal conditions.[12] Invoking the first law of thermodynamics

$$\Delta U = T\Delta S - V\Delta p = 0 \quad (22)$$

thus

$$T\Delta S = V\Delta p \quad (23)$$

Recalling eqn (15), and replacing eqn (23) in eqn (10)

$$\Delta G_r = \Delta H_r - \Delta G_{r,rev} \quad (24)$$

Then re-arranging and using eqn (13) in eqn (24)

$$\Delta G_r = \Delta H_R + nFE_{rev} = -nFE_R \quad (25)$$

Thus the enthalpy change of the reaction can be expressed in terms of voltage as

$$(\Delta H_R)/nF = -E_{EHP} - E_{rev} \quad (26)$$

then the thermoneutral potential E_{tn} can be defined as the potential at which the EHP can be operated without any heat loss or gain from the environment

$$E_H = (\Delta H_R)/nF \quad (27)$$

If the hydrogen consumption is $m'_{H_2,in}$ then the maximum current I_{max} [A] resulting from the charge transfer during the oxidation of hydrogen flowing into the EHP is

$$I_{max} = 2Fm'_{H_2,in}/M_{H_2} \quad (28)$$

where M_{H_2} is the molar mass of hydrogen, 2.01568 g mol^{-1}. Also, the amount of hydrogen transferred across the membrane $m'_{H_2,out}$[g s^{-1}] is given by the net current I_{EHP} [A] flowing through the EHP

$$m'_{H_2,out} = I_{EHP}M_{H_2}/2F \quad (29)$$

The hydrogen yield or η_{H_2} gives a measure of the efficiency of hydrogen recovery which is useful when the EHP is used to purify H_2 fed from a gas mixture and is often referred to as the separation efficiency. It can be expressed as

$$\eta_{H_2} = m'_{H_2,out}/m'_{H_2,in} \quad (30)$$

The current efficiency, η_I is a measure of how much of the supplied hydrogen contributes to the net current and is determined as

$$\eta_I = I_{EHP}/I_{max} \quad (31)$$

The current efficiency is also equivalent to the faradaic efficiency η_F defined as the ratio of net current drawn over the actual maximum current expected from the oxidation of a given amount of hydrogen oxidised over a specific time interval. The net current is the difference between the maximum attainable current and the current I_{loss} [A] lost

$$\eta_F = 1 - (I_{loss}/I_{max}) \quad (32)$$

where I_{loss} is the sum of current representing hydrogen losses *via* back diffusion across the membrane from the cathode to the anode and leakage out of the EHP *via* seals at the edges of the electrodes. For a well-designed EHP, the bulk of leakage losses comes from back diffusion across the membrane. Thus, I_{loss} can be estimated from the molar flux of hydrogen permeating through a polymeric membrane, n'_{loss}, which is determined as[13]

$$n'_{loss} = P_{H_2}A_{mem}\Delta p/\delta \quad (33)$$

where P_{H_2} [cm^3 cm cm^{-2} Pa^{-1} s^{-1}] is the permeability of H_2 through the membrane material, A_{mem} [cm^2] is the geometric area of the membrane, and δ [m] is the thickness of the membrane. Using Faraday's law,

$$\eta_F = 1 - \left[\left(P_{H_2}A\Delta p/\delta\right)/n'_{H_2,in}\right] \quad (34)$$

As shown in eqn (26), the voltage E_{EHP} required to run a real EHP is higher than the E_{rev} because of voltage drops caused by irreversible losses. These losses can be attributed to

- Activation polarisation E_{act} of the catalysts
- Ohmic losses E_{act} caused by internal resistance of the EHP
- Concentration losses E_{conc} caused by suboptimal mass transfer of H_2 or H^+ to the surface of the anodic and cathodic catalysts, respectively.

Thus

$$E_{EHP} = E_{rev} + E_{act} + E_{ohmic} + E_{conc} \quad (35)$$

The activation polarisation E_{act} is negligible because of the very fast kinetics of HOR and HER on platinum except for exceedingly low loadings around 0.003 mg pt cm^{-2} at relatively high current densities, *ca.* 3 A cm^{-2}.[14] The ohmic losses E_{ohmic} are caused by the resistance of the membrane electrolyte, R_{mem} [Ω], the supporting electrodes $R_{electrode}$ [Ω], and the catalyst layers R_{CL} [Ω],

$$E_{ohmic} = I_{EHP} \times (R_{electrode} + R_{mem} + R_{CL}) \quad (36)$$

and $R_{electrode}$ can be determined as

$$R_{electrode} = (2 \times \delta_{electrode})/\sigma_{electrode} \quad (37)$$

where $\sigma_{electrode}$ is the conductivity [S m^{-1}] of the electrode and $\delta_{electrode}$ is the thickness of the electrode [m]. For optimised platinum catalysts, the resistive losses are small compared to those of the membrane and are thus also negligible.[14] Conversely, R_{mem} can be represented by

$$R_{mem} = \rho_{mem} \times \delta_{mem}/A_{mem} \quad (38)$$

where ρ_{mem} is the resistivity of the membrane [Ω m] and δ_{mem} is the thickness of the membrane [m].

The concentration losses occur if gas mixtures are used on the anode side, such that the catalyst is poisoned and/or on the cathode, if evolved hydrogen is not rapidly removed from the catalyst surface. The concentration polarisation can be approximated by a Tafel-like behaviour of the reaction similar to when the removal of reaction product is the rate determining step as[15]

$$E_{conc} = (RT/2F)\ \ln\{1 + (I_{EHP}/I_{LIM})\} \quad (39)$$

From eqn (12), the theoretical work required for isothermal compression work is

$$W_{iso,rev} = I_{EHP}\, E_{rev} \quad (40)$$

Thus, the maximum theoretical efficiency of an EHP is related to the electrical power input to the EHP from eqn (9) as

$$\eta_{max} = W_{iso}/W_{act} = E_{rev}/E_{EHP} \quad (41)$$

This is also termed as the voltage efficiency η_E. Then the overall EHP efficiency η_{EHP} is

$$\eta_{EHP} = \eta_E \times \eta_C = (I_{EHP} \times E_{rev})/(I_{max} \times E_{EHP}) \quad (42)$$

If heat must be supplied to the EHP, the thermal efficiency η_{therm} is given by

$$\eta_{therm} = I_{EHP}\, E_{EHP}/\Delta H \quad (43)$$

Lastly, the specific electrical energy required for compression is the electrical energy supplied over a given time interval t divided by the hydrogen flux at the cathode (outlet)

$$\xi_{ele} = (E_{EHP} \times I_{EHP})/\left(m'_{H_2,out}\right) \quad (44)$$

2. Literature review

2.1. Current challenges

A key advantage of EHP over mechanical compressors is the ability to separate hydrogen from gas mixtures. During operation, only protons from the HER pass through the electrolyte membrane, while other gasses remain on the anode side. These gasses can only reach the cathode side through diffusion, resulting in reported hydrogen purities of up to 99.99% at the EHP outlet.[16] For this reason, many studies include H_2 gas mixtures as the input to the anode to simulate hydrogen separation, for example from methane pipelines.[17] H_2 concentrations as low as 10% have been successfully separated using an EHP with the remaining 90% as N_2[18] or methane/natural gas blends.[19]

The second branch of studies are focused on compressing high purity hydrogen as the feed to the anode. EHPs have an advantage over mechanical compressors because they are governed by isothermal as opposed to adiabatic compression, leading to higher theoretical efficiencies.[20–22] Multiple studies have successfully compressed hydrogen to over 100 bar,[23–25] with the highest recorded EHP pressure of 1300 bar reported from HyET Hydrogen.[26]

Water management has been identified as a key area of study of EHPs. Although not required for the HOR or HER, the membrane must be sufficiently hydrated, as ionic conductivity through the membrane is greatly hindered with an improperly hydrated membrane.[27] Water must therefore be supplied to the EHP, as it is neither produced in an EHP as it is in a PEM fuel cell (PEMFC), nor delivered as a reactant as in a PEM electrolyser (PEMEC).[17,22,28]

Back diffusion is another drawback of EHP technologies. Back diffusion is the permeation of molecular hydrogen from the high-pressure cathode to low pressure anode through the PEM. Pressure differential, membrane thickness, temperature, and water content are all factors affecting the rate of back diffusion through of the membrane. Back diffusion increases linearly with the pressure difference across the PEM.[18,27] At high cathode pressures, back diffusion becomes problematic for EHP operation as the rate of hydrogen diffusing through the membrane increases. Strobel and Chouhan concluded that the theoretical maximum achievable cathode pressure is dictated by the rate of back diffusion through the membrane.[29,30] Grigoriev was successful in reducing the back diffusion rate of a Nafion™ 117 membrane through zirconyl phosphate impregnation, but at the expense of a higher membrane resistance.[23] Hence, further research and novel membrane designs are needed to reduce the rate of back diffusion in EHPs.

Gas feed impurities, particularly CO and CO_2 are known to poison platinum catalysts at low temperatures.[31–33] Wainright *et al.* demonstrated that phosphoric acid-doped polybenzimidazole (PBI) membranes exhibit high proton conductivities at elevated temperatures.[34] EHPs utilizing phosphoric acid-doped PBI membranes have been shown to operate at elevated temperatures up to 200 °C, offering enhanced tolerance of the platinum catalyst to impurities in the hydrogen feed, including CO, CO_2, and N_2.[3,35–37] Increased phosphoric doping levels tend to enhance proton conductivity, but reduce the mechanical strength of the membrane, thereby limiting its application in current devices.[38,39] Innovative proton conducting membrane materials such as copper based metal organic frameworks (MOFs) could provide alternative high proton conductivity PEM with the flexibility to incorporate various functional groups for enhanced stability and proton conduction.[40]

Kim *et al.* studied the effect of reduced platinum loading on a high temperature PBI based EHP using varied platinum loadings of 1.1 mg cm^{-2} and 0.2 mg cm^{-2} for hydrogen separation from a 1 : 1 ratio of hydrogen–carbon dioxide mixture at atmospheric pressure.[41] All four combinations of platinum loadings were measured at 160 °C at atmospheric pressure. The reduced anode catalyst loading increased the voltage by 72% at 0.8 A cm^{-2}, while the reduced cathode catalyst loading had a negligible effect on the voltage. Beyond further exploration of platinum catalyst loading for compression of hydrogen, novel non-platinum group metal (PGM) HOR and HER catalysts are highly interesting for EHPs. A bismuth based MOF has also been demonstrated as a stable catalyst in acidic environment for use in CO_2 reduction reaction in a PEM electrolyser.[42] Cobalt oxide based catalysts mixed with Vulcan have been shown to outperformed platinum as an HER catalysts in a PEM electrolyser at voltages above 2.3 V.[43] A molybdenum carbide aerogel HER catalyst is currently the only reported non-PGM catalyst tested in an EHP. The catalyst exhibited a fully recoverable voltage loss after a 180 hour stability test at current densities up to 3 A cm^{-2} in a PBI-based EHP for hydrogen separation.[44] Such novel non-PGM catalysts should be further explored in EHPs to reduce dependence on platinum-based catalysts.

In literature, only a few studies have investigated long term operation degradation of EHPs and their mechanistic pathways.

Possible degradation mechanisms include loss of active catalyst surface area due to absorbed species in the anode inflow, mechanical damage of the membrane during operation, and carbon corrosion of electrodes.[45] A 1000-hour durability test was conducted by Sustainable Innovations LLC, to demonstrate that the EHP could operate under dynamic voltage cycling; however, at present standardized durability procedures do not exist for EHPs.[46]

The MEMPHYS project also reported durability measurements of a 5-cell stack over three month testing period using a combination of steady-state operation and an accelerated stress test adapted from PEMFC testing.[47] No significant EHP component degradation was observed. In fact, variations in the operating conditions were found to have a larger impact on performance than degradation. They also concluded that for optimal durability the humidification should be adapted for each specific operating point depending on operation conditions. The development of accelerated stress testing procedures is needed to better understand degradation mechanisms and long-term durability of EHPs.

2.2. Experimental setups and testing

The experimental setup used for studying EHP varies depending on the intended application; compression and separation of hydrogen are the focus of most EHP experiments. For example, EHPs have been used with pure hydrogen feeds for recirculation of H_2 for fuel cell stacks.[48,49] They have also been used in more niche applications, such as in combination with liquid organic hydrogen carriers to increase the rate of dehydrogenation and produce compressed pure hydrogen,[50] and have modelled for driving a metal hydride based heat pump.[51] Typical EHP test cells have a zero-gap form factor. A 3D printed tubular EHP constructed by Zängler *et al.* which operated at 60 mA cm^{-2} at a differential pressure of 2 bar was the only exception found in literature.[52] The purpose of the study was to offer proof of concept for better surface to volume ratios for EHP designs.

Nordio developed a test setup using a 50 cm^2 EHP manufactured by HyET Hydrogen.[17] Both pure hydrogen and mixtures containing methane, nitrogen, hydrogen, helium and carbon dioxide contaminants were measured. Gas flows were controlled by electronic valves connected to mass flow controllers. The gas flows were fed into a humidification bottle containing de-ionized (DI) water to humidify the gas feed to the anode. The gas temperatures are heated with tracing lines before humidifying the gas flows by bubbling through distilled water heated with a magnetic hotplate stirrer. On the cathode side, the outlet gas was sent through a condenser containing ice before passing through a flow meter. The cathode pressure was controlled with a manual back pressure regulator. The study found that 100% H_2 could be collected at the cathode when using nitrogen and methane as a contaminant and a purity of 98% was achieved using helium.

Separation of the HOR and HER losses in an EHP can be challenging because both reactions proceed rapidly in the presence of a platinum catalyst in a PEM based system. Hao *et al.* found that the HOR followed the Tafel–Volmer route while the HER followed the Volmer–Heyrovsky route by separating the HER and HOR in an EHP using a platinum reference electrode integrated into an EHP. HER losses were found to be larger than for HOR, while the HER losses decreased with increasing cathode pressure from 1 barg to 10 barg and were attributed to an increase in the coverage of absorbed hydrogen on the catalyst surface.[53] Stühmier *et al.* studied the pressure dependence of HOR/HER reactions in an EHP by using a relatively high Pt catalyst loading (0.4 mg cm^{-2}) on the counter electrode, which also serves as the reference electrode, and a very low Pt catalyst loading (1.2–1.6 μg cm^{-2}) on the working electrode.[54] They found that both HOR and HER follow a Tafel–Volmer mechanism at pressures up to 450 kPa and temperatures to 90 °C. They also observed that the HOR approaches a limiting current proportional to the hydrogen pressure at high current densities. However, it could not be determined whether this was due to a rate limiting Tafel reaction or mass transport of H_2 through the ionomer layer.

A setup to study water transport along the length of a 30 cm^2 EHP electrically segmented into 20 sections for studying H_2 compression to 32 bar was developed by Sdanghi.[20] The EHP was heated using circulated hot water which flowed in separate channels in the EHP. H_2 passed through a flow controller before being bubbled through DI water to humidify the inflow to the anode. Unreacted H_2 was collected at the anode outlet and its humidity measured. The cathode inlet was closed and the flow from the outlet passed through a condenser then through a pressure regulator. All gas lines were heated to 75 °C to prevent condensation and a separate heating line was used to control the cell temperature. The study showed that membrane dehydration decreased from 90% relative humidity (RH) to 55% RH along the anode and emphasized the importance of proper membrane hydration for optimal EHP performance.

Grigoriev developed a 25 cm^2 EHP utilizing a gas humidifier and a gravity-fed liquid water humidifier, which was tested at stable pressures up to 48 bar between 35 °C and 75 °C.[23] The EHP consisted of 316L stainless steel flanges used to compress end plates, fluorine rubber gaskets, porous carbon anode gas diffusion layer (GDL), porous titanium anode GDL, and a titanium mesh. The MEAs consisted of a Nafion™ 117 membrane with carbon supported platinum catalysts, with equal loadings on anode and cathode of 0.4 mg cm^{-2} Pt and 0.8 mg cm^{-2} Pt. Sigracet 10bb carbon paper with a microporous layer (MPL) was used as the anode GDL, porous titanium was used as the cathode GDL, and titanium meshes were used to support both GDLs. Using the setup, H_2 was compressed from 1 bar to 48 bar at a current density of 0.2 A cm^{-2} and 140 mV at 75 °C. It was found that using a single EHP stable operation could be achieved up to 48 bar, however over 50 bar, the use of two or more compressors is recommended to prevent gas excessive leaks. Hao *et al.* also used a setup employing an internal liquid humidifier on the cathode, but used a dry dead-end anode configuration.[55] The study utilized a 5.3 cm^2 EHP cell to compress hydrogen from atmospheric pressure at varying

Table 1 Notable experimental setups reported in the literature, including efficiencies and performance metrics measured at specific operating points and under defined conditions

Author	GDE geometric area [cm^2]	Membrane	Voltage efficiency [%]	Voltage at 0.5 A cm^{-2} [mV]
Grigoriev[23]	25	Nafion™ 117 (183 μm)	—	~175 (75 °C, 0 barg)
Pineda Delgado[56,57]	5	Nafion™ 115 (127 μm)	—	212 (30 °C, 10 barg, 100% RH)
			—	278 (80 °C, 10 barg, 100% RH)
Sdanghi[20]	30	Nafion™ XL (28 μm)	—	~95 (60 °C, 32 barg)
		Nafion™ 117 (183 μm)	—	~240 (60 °C, 32 barg)
Hao[55]	5.3	Nafion™ 117 (183 μm)	17 (60 °C, 20 barg, 0.5 A cm^{-2})	~365 (30 °C, 20 barg)
			10 (30 °C, 20 barg, 0.5 A cm^{-2})	~200 (60 °C, 20 barg)

EHP temperature setpoints to 2 MPag. The EHP contained a Nafion™ 117 membrane with 0.2 mg cm^{-2} Pt catalyst loadings for both anode and cathode. Sintered stainless steel and carbon cloth (EC-CC1-060T) were used as double GDLs on the anode with the same sintered stainless-steel sheet with a carbon paper (24AA) used on the cathode. The flow field plates were constructed from 316L stainless steel. The high frequency resistance was measured at 10 kHz at each measurement setpoint to estimate the series resistance of the cell. The setup operated at 0.5 A cm^{-2} at 123 mV with a hydrogen flow rate at the anode of 40 ml min^{-1} with 0.5 MPag cathode pressure at 333 K. A summary of notable experimental setups outlined in the literature including performance metrics is provided in Table 1.

Despite recent progress, several key challenges remain for EHPs. Maintaining optimal membrane humidification - particularly at high current densities – is critical for ensuring high proton conductivity in low-temperature PFSA-based membranes, while improving the balance between of mechanical strength and proton conductivity remains a key challenge for high-temperature PBI-based membranes. Further research is needed to identify membranes that offer high proton conductivity while supressing hydrogen back diffusion through the membrane, which limits overall efficiency for compression. In addition, there is a significant lack of long-term studies addressing catalyst degradation mechanisms and stability. Studies in literature use platinum-based catalysts for both the HER and HOR, underscoring the need to explore alternative non-PGM catalysts that can deliver similar performance and durability at a lower cost, thereby reducing reliance on expensive rare earth metals. Additionally, the absence of standardized testing procedures and operating conditions hinders the comparability of EHP studies. Establishing standard testing procedures is essential for meaningful comparisons across the field.

3. Development of an electrochemical hydrogen pump and test rig for academic labs

This section aims to provide details of our EHP test rig developed and used at Helmholtz-Zentrum Berlin, so others entering or working in the field can use the information to develop their own EHP testing stations. We will discuss key requirements for an EHP test station and provide information on the components of our rig including materials used and vendors. The experimental testing procedure and an example of key performance data are included as a guide for establishing an EHP test setup. A troubleshooting guide and a description of best practices, both provide insights for safe, reliable and consistent operation.

Despite EHPs generally having the same zero-gap form factor as a PEMFC or PEMEC, the objective of using an EHP to compress hydrogen at the cathode inevitably leads to varied test setup requirements. These differences in the requirements for the EHP setup are summarized as follows:

1. Mechanically strong materials for the EHP test cell are required to manage high cathode pressures.

2. The absence of oxygen reactions allows the use of oxidation-prone materials (*i.e.* titanium and gold coatings are not necessary), and low platinum loadings are sufficient as neither oxygen reduction reaction (ORR) nor the oxygen evolution reaction (OER) are present in EHPs.

3. Water required for membrane hydration but is neither a product or reactant as it is for PEM fuel cell or electrolyser, respectively.

4. EHP operating voltage (approximately 0.05–0.5 V) is generally lower than that of a PEMFC or PEMEC, reducing the likelihood of oxidation of carbon gas diffusion electrodes (GDE).

3.1. Description of test rig

3.1.1. Flow control and measurement. To the best our knowledge, there are no commercial EHP test rigs currently available. The following description shall thus serve as a guide to any laboratory wishing to establish EHP testing capabilities. The test rig described in this study was designed for hydrogen compression studies. It could, however, be easily adapted for H_2 separation measurements by adding an additional gas source and flow controller to the anode inflow. Fig. 2 presents a photograph of the EHP test rig, highlighting the general layout of the instrumentation and the location of the EHP. More detailed information on the test rig's electronics specifications and individual test cell components can be found in the NOMAD database.

Fig. 3 shows schematic diagrams illustrating (a) the locations of key fluid flow and temperature control/measurement components within the system, and (b) the fluid flow paths during normal EHP operation. The only fluid inflow to the EHP is a humidified hydrogen steam to the anode inlet. Hydrogen was humidified to 100% RH using a controlled evaporator

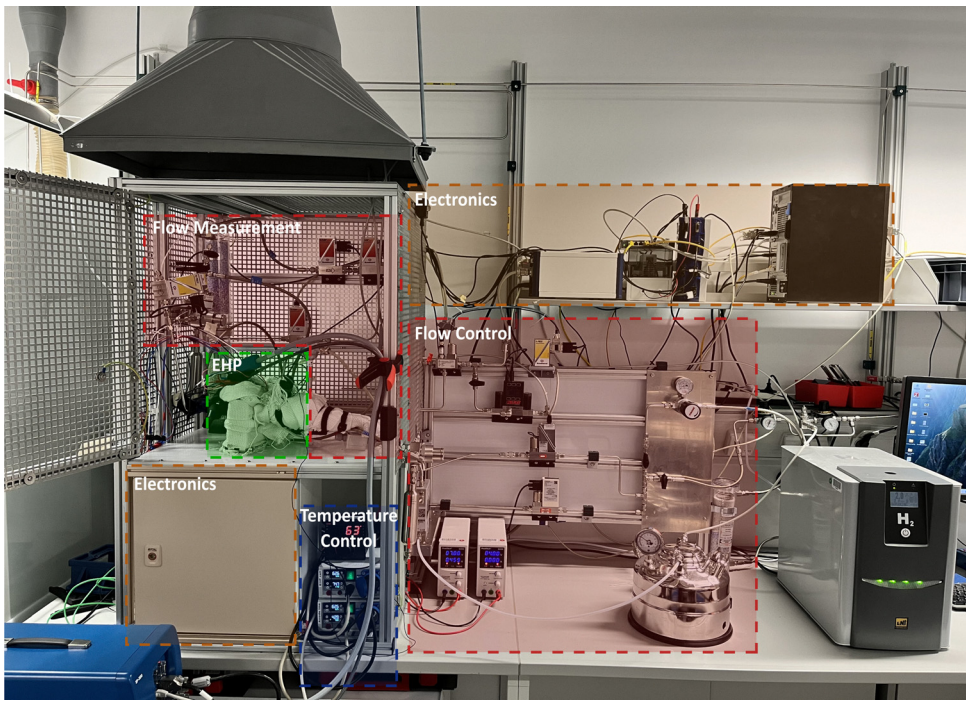

Fig. 2 Overview of the test rig used for EHP experiments. Key components including the EHP (thermally insulated), flow measurement and control systems, temperature control units, and supporting electronics are highlighted.

mixer (CEM) (Bronkhorst® CEM Evaporator). A hydrogen generator (LNI Swissgas H_2 Basic) supplies H_2 pressurized to 2.0 barg to the gas inlet of the CEM and a pressurized water vessel (MilliporeSigma™ XX6700P01) filled with 18.2 MΩ ultrapure water (Barnstead™ Smart2Pure™ Pro) is pressurized to 1.5 barg using a nitrogen gas blanket. Water flow is controlled using a Coriolis flow meter (Bronkhorst® mini CORI-FLOW™) and gas is controlled using a thermal mass flow controller (Bronkhorst® EL-Flow®). Stainless steel piping with an outer diameter of 6 mm was primarily used for fluid connections. Flexible stainless steel braided PTFE lined hose (Swagelok® SS-4MBHT-24) was used to make connections to the EHP anode inlet and outlet easier when connecting the EHP to the test rig. Transparent PTFE tubing on the anode line connecting the pressurized water vessel to the Coriolis flow meter was used to view any bubbles in the water flow for diagnostics. Humidity is not a directly controllable parameter. The flow rates for H_2 and water at the setpoint measurement conditions were determined using Bronkhorst® Fluidat® software. A humidity sensor (Galltec Mess - und Regeltechnik GmbH + Mela Sensortechnik GmbH – CVR2.D/5) was installed upstream of the EHP to verify the RH of the inlet flow to the EHP anode. The humidity sensor was placed in an in-house manufactured stainless steel block adaptor to allow for inline RH monitoring. Two 20 W heating pads were attached to the humidity sensor block, which was wrapped in thermal insulation tape and connected to its own PID temperature controller to ensure that the sensor temperature remains near the setpoint for accurate RH measurements. Heating cuffs (Scribner LLC) were attached to the anode inlet and outlet fittings in the gap between the end of the line heating element and the EHP.

The high-pressure cathode side is of particular importance since H_2 at the cathode will be pumped at relatively low flow rates. To accurately characterize the EHP performance during pressurization, the test rig incorporates a dome-loaded pressure regulator at the cathode. The dome-loaded pressure regulator is a critical part of the test rig that ensures that the pressure of the cathode can be increased without losses through the regulator, allowing for the accurate determination of the faradaic efficiency, a key performance indicator of the EHP. The dome-loaded pressure regulator has a diaphragm made of a ridged sealing material, in this case polyetheretherketone (PEEK). Above the diaphragm, a pilot pressure is supplied using nitrogen, which pushes on the top of the diaphragm to act as a seal until the cathode pressure exceeds the pilot pressure, at which point the diaphragm bends to allow flow to pass. Downstream of the pressure regulator is a coalescence filter (Swagelok® Coalescing Filter - SS_FCE) used to remove bulk H_2O and then a desiccant column (W.A. Hammond Drierite Co., Ltd - Indicating Drierite™) removes any remaining water vapour in the H_2. This is crucial to ensure accurate mass flow meter measurements since the measurement relies on the density of the gas for accurate measurement.

3.1.2. Software and electronics. The test rig is controlled and monitored by two programs, one a self-made LabVIEW-based software and the other one EC-Lab®, which is the official BioLogic software. The former controls all other devices including humidity sensor, temperature sensors, mass flow sensors and controllers as well as pressure sensors and controllers. The latter one controls the potentiostat and the electrochemical testing.

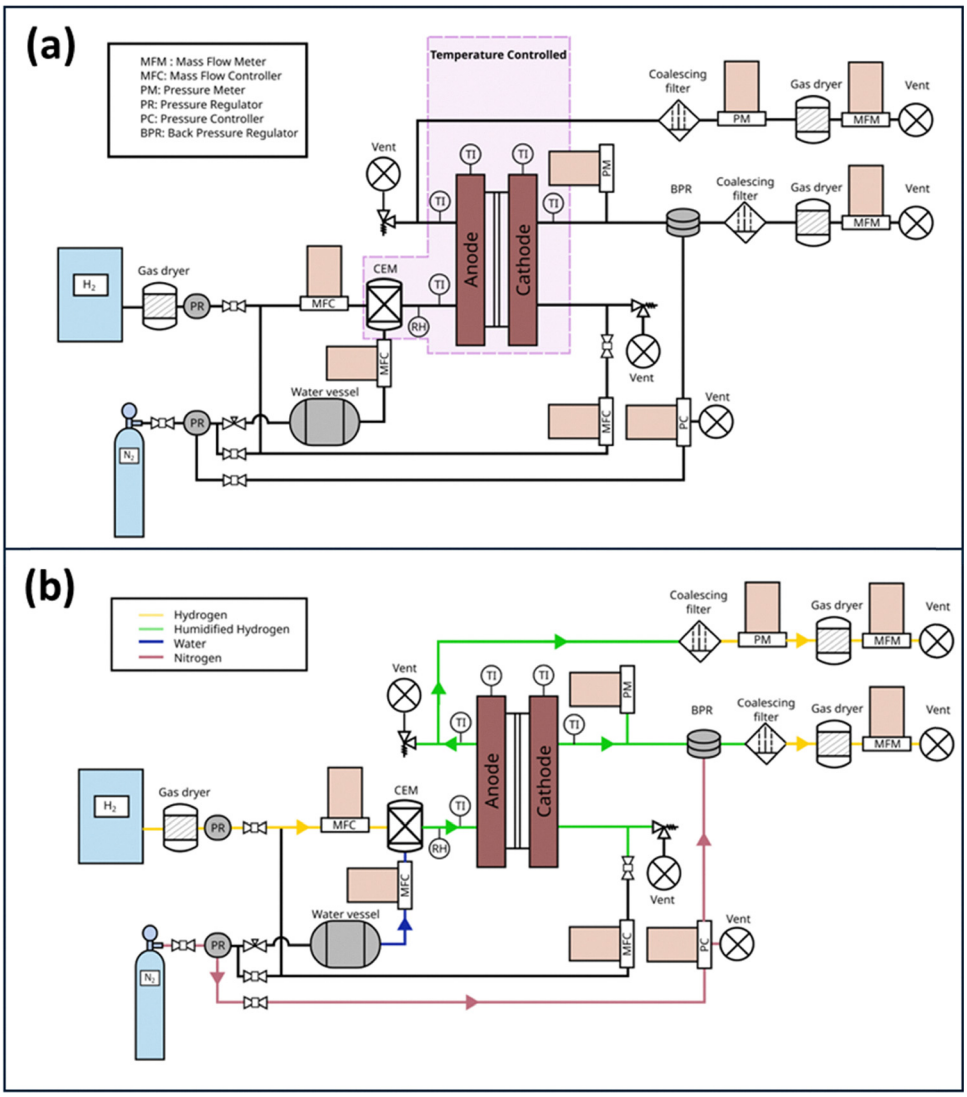

Fig. 3 Schematic diagrams of the EHP test rig. (a) Fluid connections and locations of flow and temperature control/measurement components. (b) Illustration of the fluid flow paths during standard EHP operation, showing the routing of hydrogen, nitrogen, water and humidified hydrogen streams through the system.

The LabVIEW-based software handles most of the test rig's devices and an overview of its functionalities is given in Fig. 4. It collects their data and logs it to the PC. The data is presented in multiple graphs and as a raw data table to the user. This way the performance of the electrochemical cells can be analysed in real time. The settings of all devices are done with a csv. file listing all necessary parameters to connect to the correct devices. This allows for the use of the same software on multiple test rigs without changing the actual software, but just by loading different settings files. One Virtual Interface (VI), equivalent to a subroutine in text-based programming languages, checks all data against limits set by the user and warns *via* the interface if any value exceeds its respective limit. This can automatically result in the change to a safe state for some instruments, like setting certain gas flows to zero.

Hardware fuses are integrated into the test rig to power down critical devices in case of unsanctioned operating points or in case of an emergency. Those devices are the BioLogic potentiostat, as the main power source for the EHP operation, as well as the heating units that set the pump cell to the wanted temperature. For fluid safety, pressure relief valves are installed. The hydrogen generator that provides the low-pressure inlet H_2 to the test rig is coupled to an H_2 safety sensor located above the rig and is shut down by that sensor in case of a gas leak.

3.2. Construction of electrochemical hydrogen pump

3.2.1. Material selection. In most studies of low temperature electrochemical hydrogen compression, unmodified commercial perfluoro sulfonic acid (PFSA) membranes are used as a solid electrolyte. Nafion™ is most commonly used in EHP studies.[58] Other PFSA membranes are however suitable for EHP compression and separation, including Fumasep®, Aquivion®, and Gore-Select®. The main consideration for

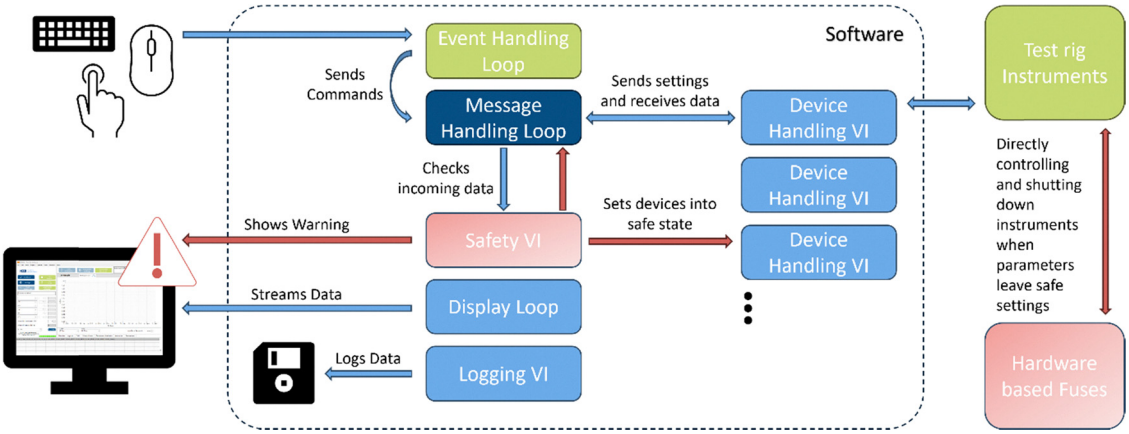

Fig. 4 Flow diagram of the software used for the test rig, providing an overview of the key functionalities and its interactions with the computer, peripheral devices, and the rig's sensor hardware.

membrane selection for hydrogen compression is the thickness. A thicker membrane will be more robust and have a lower rate of back diffusion but will have lower proton conductivity.

In this case study, a commercial 5-layer membrane electrode assembly (MEA) with carbon supported platinum (30 wt%) catalyst with a geometric area of 25 cm^2 was purchased from The Fuel Cell Store. The MEA is composed of a Nafion™ 115 membrane (127 μm) with a 410 μm carbon cloth containing a microporous layer (CT W1S1011) with Pt loadings of 0.25 mg cm^{-2} for each electrode. One side of the GDL is hydrophobic (5 wt% PTFE) to minimize flooding, while the other has a microporous layer (MPL) to reduce contact resistance between the catalyst layer and GDL, and to enhance membrane hydration. 316L stainless steel was selected for the FFP and end plates because it provides high mechanical strength, is cost effective, and chemically resistant to corrosion. Stainless steel has also been selected by others studying electrochemical compression of hydrogen.[23,55,56,59] Some studies have also investigated the use of materials with increased corrosion resistance, namely titanium and molybdenum,[59,60] but these materials significantly increase EHP costs. Table 2 provides an overview of the components of the EHP test cell along with their corresponding materials.

3.2.2. EHP test cell. An in-house designed and manufactured EHP was constructed for this case study, with a detailed view of all its components shown in Fig. 5(a). The drawing files including all dimensions for the EHP is provided in the NOMAD database. The EHP has a zero-gap configuration commonly employed for PEM fuel cells and electrolysers. Flow fields were milled into the plates to uniformly distribute the product and reactant hydrogen over the 25 cm^2 geometric area where the reactions occur. The EHP test cell employed a double serpentine flow field with 2 mm-wide channels, as shown in Fig. 5(b), with the assembled cell shown in Fig. 5(c). Silicone gaskets with a thickness of 0.5 mm (Reichelt Chemietechnik GmbH + Co – Thomaplast® Silicone Plate) were used to seal the MEA, to prevent leaks between the flow field plates and end plates, and to electrically insulate the end plates from the rest of the test rig. The gaskets were laser cut to size using a Keyence UV Laser Marker (MD-U1020C). Other typical sealing materials found in PEMFCs, namely EPDM and PTFE, have also been successfully tested in the EHP.[61] Porous 316L stainless steel supports (Bekaert Bekipor 10AL3) provided mechanical reinforcement to the MEA. They were cut to 56 mm × 56 mm and 53 mm × 53 mm and placed on the anode and cathode, respectively. Different sizes of stainless-steel supports prevent pinching of the membrane, particularly at the corners of the supports. The EHP was designed with separate end plates and FFPs allowing testing of different FFP designs and sizes. The cell assembly was performed using a three-step method to gradually increase the torque from 1 Nm to 5 Nm and finally to 10 Nm, using eight M8 bolts. Fluid connections were placed on the outside faces of the end plates and sealed with Viton™ O-rings. 1.2 mm holes were drilled in the top of the FFPs to allow for a 1.0 mm PT100 sensor (CCPI Europe Ltd.) to extend 5 cm into the FFP to measure the temperature near the middle of the FFP. Custom 50 W heating pads were manufactured by TFP Technology with holes for the fluid fittings and placed on the outside of the end plates using a temperature resistant adhesive. The heating pads are the same size as the FFPs to provide even heating and reduce the likelihood of hot spots. A temperature controller (Juchheim GmbH & Co. KG - LTR 2500-S) controls the EHP temperature using a PT100 sensor while the

Table 2 Materials used for EHP test cell components

Component	Material
Flow field plate	316L Stainless steel
End plate	316L Stainless steel
M8 Hex socket cap bolts	304 Stainless steel
Washers	316 Stainless steel
Spring washers	Carbon steel
Gaskets	0.5 mm silicone
O-rings	Viton™
M10 × 6 mm tube fittings	316 Stainless steel
MEA	0.25 mg cm^{-2} 30 wt% Pt on Vulcan/ electrode, Nafion™ 115 membrane

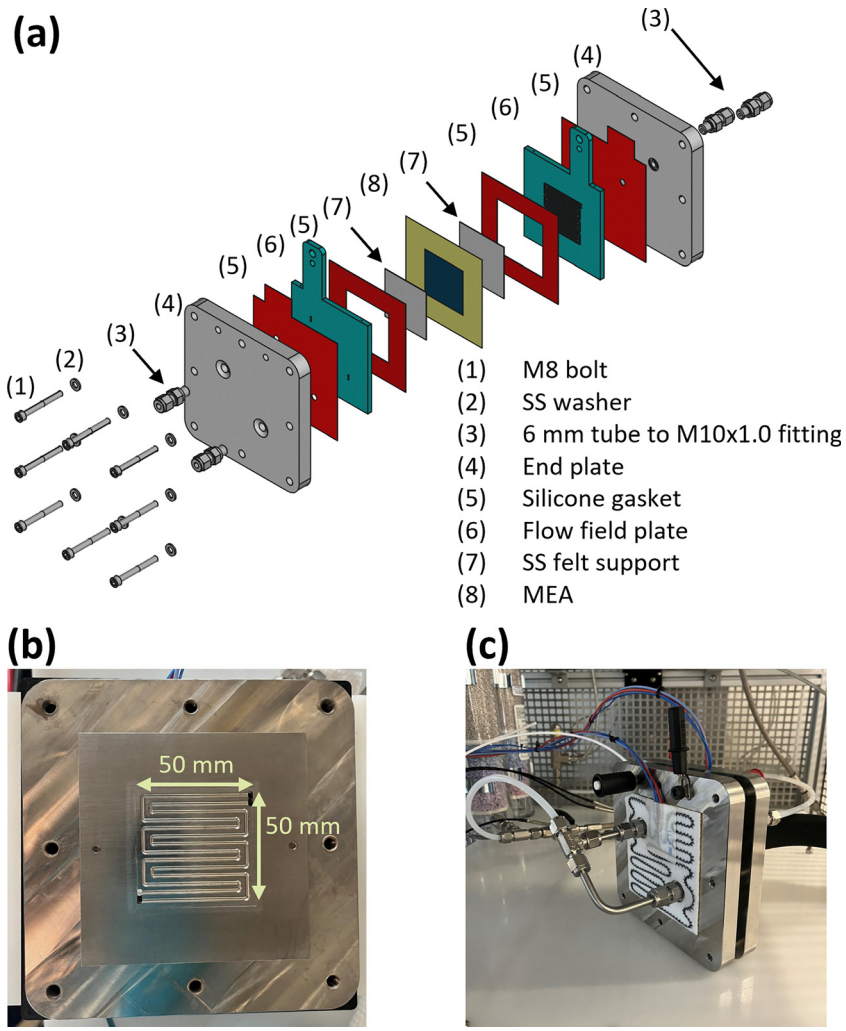

Fig. 5 (a) Detailed view of the EHP showing all components of the test cell; (b) and (c) photographs of the 25 cm^2 double serpentine flow field plate design and the fully assembled EHP, respectively.

anode and cathode temperatures are recorded with separate PT100 sensors placed in the FFPs. Each heating pad contains a PT100 sensor attached to the heating pad which is used for the safety shutoff for the temperature controller. The cell was then wrapped in a thermal insulation tape (Horst BCTEX™ Fabric Tape). The FFPs also act as current collectors for the EHP, with a section extruding vertically out of the cell that includes two holes for sense and power electrical connections using 4 mm banana sockets. Temperatures at the EHP inlet and outlets are measured inline using PT100 sensors (ES Electronic Sensor GmbH - SW Pressure Resistance Thermometer) integrated into the 6 mm stainless steel pipe using T-fittings.

3.3. Break-in and measurement procedure

As with PEM based fuel cells and electrolysers, the EHP requires a break-in procedure before measurements can be performed. The purpose of this step is to remove impurities on the catalyst surface, improve the utilization of the catalyst and to hydrate the membrane.[62,63] Break-in procedures are not commonly reported in the literature for EHP. Pineda-Delgado reported break-in by operating the cell as a PEM fuel cell at 30 °C and 80 °C and RH of 50% and 100% before switching to EHP operation.[56] Zou reported using a break-in procedure borrowed from fuel cell procedures where the voltage was increased from 0.05 V to 0.6 V in steps of 0.05 V held for 2 minutes.[64]

The experimental procedure in our case study has been adapted from PEMFC break-in procedures and collective experience in EHP testing.[62,65,66] The experimental procedure for conducting EHP experiments is summarized in Table 3. This procedure is intended to serve as an initial standardized approach to benchmarking EHP performance. Break-in was conducted at 75 °C and the EHP characterization was conducted at 60 °C. Humidified hydrogen with an RH of 100% was supplied to the anode during both steps. The gas supply line carrying humidified hydrogen to the EHP was heated to 2.5 °C above the EHP setpoint temperature to prevent condensation in the piping.

Following cell assembly, the EHP was connected to the test setup and purged with N_2 for 10–15 minutes to clean the lines and remove air from the lines. The plug valve on the cathode line was opened to allow gas to flow through the cathode side of

Table 3 Experimental procedure for EHP testing using a BioLogic SP-300 potentiostat

	Step	Purpose	Description/Technique
1	Purge	Clear lines of any residual air after EHP installation in the test rig	10–15 minutes of purging with N_2 • 100 mln min^{-1} anode • 100 mln min^{-1} cathode
2	Warm up	Allow EHP to come to temperature and apply humidified inflow until stable	200 mln min^{-1} H_2 at 100% RH EHP temperature 75 °C 50 mln min^{-1} H_2 at cathode for 10–15 minutes prior to break in
3	Pressurization	Operate EHP to bring cathode to set pressure (5.0 barg)	CP at 0.1 A cm^{-2} for 30 minutes
4	Break in	Voltage cycling to prepare EHP for characterization measurement at 75 °C	(1) CP at 0.2 A for 60 minutes (2) Stepped CA looped 5 times • 130 seconds at 0.05 V • 130 minutes 0.2 V (3) Sequence repeated 20 times
5	Performance characterization	Collect data for a polarization plot using CP measurements held for five minutes followed by a quick GEIS scan to determine HFR	EHP temperature 60 °C (1) CP at 8 mA cm^{-2}, 10 mA cm^{-2}, 12 mA cm^{-2}, 20 mA cm^{-2}, 50 mA cm^{-2}, 100 mA cm^{-2}, 200 mA cm^{-2}, 300 mA cm^{-2} and 400 mA cm^{-2} (2) Frequency range: 1000 Hz to 1 Hz Voltage amplitude: 10 mV • 8 data points per decade • 6 data points per frequency
6	Diagnostics	EIS scan over larger frequency range to obtain EIS spectra	GEIS at 50 mA cm^{-2}, 100 mA cm^{-2}, 200 mA cm^{-2}, 300 mA cm^{-2} • Hold at setpoint: 5 minutes • Frequency range: 1000 Hz to 20 mHz • Voltage amplitude: 10 mV • 8 measurement points per decade • 6 measures per frequency

CP: chronopotentiometry, CA: chronoamperometry, GEIS: galvanostatic electrochemical impedance spectroscopy

the EHP through the FFP to the surface of the MEA. The EHP was then heated to 75 °C while humidified H_2 flowed to the anode side to humidify the membrane. When the EHP reached the setpoint temperature, H_2 was run through the cathode line to remove N_2 from the cathode line. The break-in procedure was conducted at a cathode pressure of 5.0 barg. Thereafter, the H_2 supply to the cathode was shut off and the plug valve on the cathode line was then closed. The EHP was operated at 0.1 A cm^{-2} for 30 minutes to allow the cell to pressurize. The break-in procedure for the EHP was then conducted by operating at 0.2 A cm^{-2} for 60 minutes, then cycling between voltages of 0.05 V and 0.20 V held for 130 seconds and repeated five times. This entire sequence was then repeated a total of 20 times to break in the MEA.

The operating conditions used in this sample experimental measurement are summarized in Table 4. The performance of the EHP was measured using a stepped chronopotentiometry (CP) to produce a polarization plot. The EHP current was held for 5 minutes at each step. Short galvanostatic electrochemical impedance spectroscopy (GEIS) measurements were taken from 1000 Hz to 1 Hz after each step to determine the high frequency resistance (HFR) during operation. Additional GEIS measurements, ranging from 1000 Hz to 20 mHz, were also conducted at 50 mA cm^{-2}, 100 mA cm^{-2}, 200 mA cm^{-2} and 300 mA cm^{-2} to measure a complete Nyquist plot, which can be compared for diagnostic purposes. Reproducible EIS results provide a reliable diagnostic metric for healthy system operation, however limited EIS data has been reported in literature for

Table 4 Operating conditions set during measurement of the example results presented in the case study

Parameter	Set value
Anode H_2 flow	200 mln min^{-1}
Anode line temperature	62.5 °C
Anode H_2O flow	1.166 g h^{-1}
CEM temperature	62.5 °C
Cathode pressure	5.07 barg
Anode pressure	Atmospheric

EHPs.[16,53,55] Fig. 6(a) shows a plot of the transient EHP data collected during the stepped CP measurement. The electrochemical performance of the EHP is shown in the polarization plot in Fig. 6(b). The current efficiency in Fig. 6(c), was calculated using the measured H_2 flow at the cathode and EHP current using eqn (31). A small reduction in the measured cathode pressure was observed with decreasing current and corresponding cathode flow. This is inherent to the back pressure regulator's operation and the differences diminish with increasing flow rate at the cathode. The EHP setup exhibits high current efficiency at a pressure of 5 barg indicating good sealing and a low rate of back diffusion though the membrane. Operating the EHP initially at a low pressure minimizes the back diffusion effects and provides a good starting point for determining if leaks are present in the system. This measurement guide, along with the example data set obtained under the operating conditions listed in Table 4 is intended to serve as a reference for EHP measurements. The accompanying

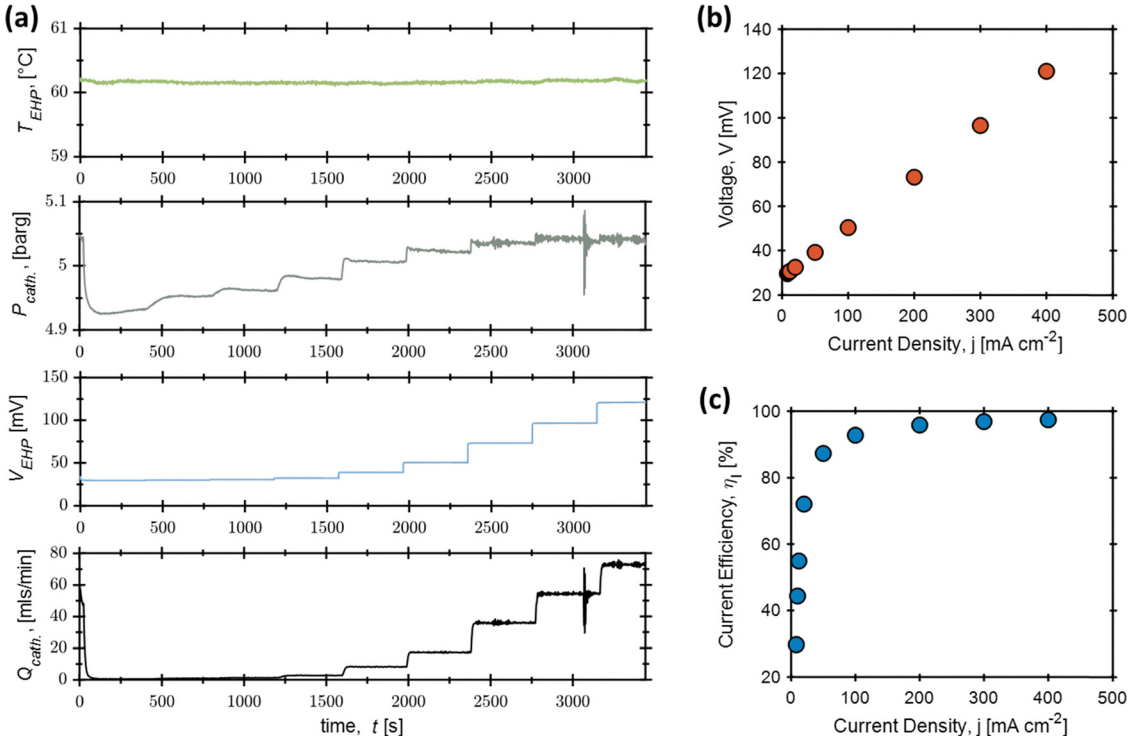

Fig. 6 (a) Transients of EHP data (T_{EHP} EHP cell temperature, $P_{cath.}$ pressure at the cathode, V_{EHP} cell voltage and $Q_{cath.}$ hydrogen volumetric flow rate at the cathode) measured during the performance characterization step of the measurement procedure, in which CP measurements of 5 minutes are performed. The resulting polarization plot produced from the CP measurements is plotted in (b). The current or faradaic efficiency relating the measured hydrogen gas flow from the cathode is plotted in (c).

troubleshooting guide is provided to help identify and resolve issues encountered during measurements.

3.4. Troubleshooting: challenges and solutions

The difficulties in operating the EHP typically come from the elevated pressure at the cathode. We found that having no supports on the MEA caused the membrane to be pushed into the flow field, causing it to puncture. The addition of stainless-steel supports on both anode and cathode can solve this issue, but having the same sizes caused pressure points at the corners which also caused the membrane to puncture. Supports that are too close in size to the flow field are also prone to being pushed into the flow field if there are any small misalignments when the EHP is pressurized as shown in Fig. 7. The effect of cell compression is of particular importance for EHP operation because as the cathode pressure increases the pressure tends to push the MEA components towards the anode. At unpressurized or low-pressure conditions (<5 barg) this will materialize as a slightly higher ohmic resistance, but at higher pressures excessive stretching of the membrane can lead to a membrane puncture.

Separating the losses associated with the HOR and HER during EHP operation is challenging. In a PEM fuel cell, the contribution of HOR related losses using a platinum catalyst has been reported to be less than 10 mV when the catalyst loading is reduced from 0.4 to 0.05 mg cm^{-2} at a current density of 1.0 A cm^{-2}.[67] A better understanding of catalyst behaviour is important, particularly as studies on long term catalyst stability are scarce in the literature.

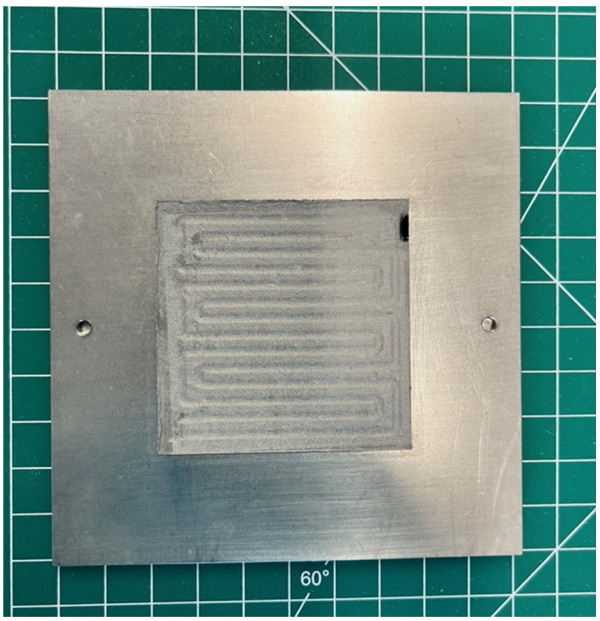

Fig. 7 Stainless steel support that was pushed into the anode FFP, causing the membrane to puncture.

EHP performance is highly sensitive to the level of humidification. Since water is neither a product nor reactant for HER

and HOR, it must be supplied to the membrane. Insufficient humidification can cause instability and increases in the EHP voltage, mainly *via* increased membrane resistance.[20,56] Water management is typically accomplished through humidifying the anode inflow to the EHP, although Hao *et al.* also reported the use of a liquid water humidifier on the cathode.[55] Zou *et al.* have also reported membrane failure through H_2 starvation which caused the EHP voltage to increase rapidly, burning the surface of the MEA.[64] We recommend monitoring RH using an in-line humidity sensor to ensure the EHP is properly humidified during measurements. Applying safety limits to the potentiostat can also prevent EHP operation above specified voltage limits, preventing rapid heating caused from voltage spikes if hydrogen starvation occurs, preventing damage such as delamination to the MEA. Understanding long term causes and severity of membrane degradation remains a challenge for the long-term operation of EHPs. In particular, insights on the combination of mechanical stress and chemical aging during high pressure operation and the effect of impurities in the inflow, particularly for hydrogen separation, remain elusive. Long-term studies investigating the rate of hydrogen back-diffusion and ionic conductivity through the membrane are also needed to understand operational lifetime under different operating conditions. Degradation studies are essential to characterize the mechanisms affecting the catalyst and catalyst support, and to assess their impact on proton and electron transport over time.

4. Conclusions and perspectives

In this work, we reviewed the emerging field of electrochemical hydrogen pumps, which enable efficient hydrogen compression and separation from mixed gas streams. An overview of experimental setups from the literature and a case study detailing an electrochemical hydrogen pump test setup are presented. A testing procedure and an example of the data that can be recorded with this setup are used as a baseline for EHP testing. We offer a basic troubleshooting guide to assist in establishing an operable testing setup. The establishment of a universal testing procedure for EHPs is critical for proper comparison between studies and is currently lacking in literature. Additionally, very few tests on the long-term durability tests of EHPs have been conducted. Since EHPs are used for a variety of applications, it is preferable to establish testing procedures without the use of specialized equipment or need for excessive capabilities, such as operating at high cathode pressures or handling multiple gas inflows. Ideally, pure hydrogen should be used as a benchmark, also when evaluating EHPs for the purpose of hydrogen separation.

We have also identified areas requiring further development to enable the widespread deployment of EHPs. Firstly, the use of novel catalysts based on non-critical materials, as well as alternative membrane materials, remains largely understudied. While most existing studies focus on the effect of operating conditions on EHP performance, there is significant untapped potential in exploring new materials within EHP technology.

Although electrochemical hydrogen pumps have the potential to achieve higher operating pressures, exceeding the current state-of-the-art is not an immediate priority; instead, research should focus on improving long-term stability and understanding performance changes over extended operation to ensure reliable operation. Current studies on EHPs lack long term testing and accelerated stress testing, leaving the present maximum operational lifetimes and the effect of degradation of the membrane and catalysts is widely unknown. Long term degradation studies of an EHP require further study to better understand these degradation mechanisms.

In relation to the chemical degradation of catalysts and membrane components during operation or post-mortem, various techniques/methods can be implemented from the electrolyser or fuel cell fields already used in academic laboratories.

For post-mortem analysis of catalysts on the GDLs, X-ray photoelectron spectroscopy can be utilized to detect the oxidation of the Pt catalysts by fitting the spectrum in the Pt core level regions and detecting shifts in the binding energies.[68] Currently the field of electrochemical H_2 pumps is dominated by using Pt based catalysts, as it is the state of the art for HER and HOR, however if catalyst development to more inexpensive earth abundant catalyst (Ni, Mo, Mn, Co, *etc.*, with or without Pt) would be foreseen within the electrochemical H_2 pump community, XPS would be an extremely valuable technique as it is routine in the electrolyser field to detect changes in these earth abundant elements to help in catalysts development.[69] Furthermore, post-mortem X-ray absorption spectroscopy can be utilised on the catalysts before and after operation to monitor changes in the oxidation state by developing a calibration curve of known materials during the same beamline session.[70] Raman spectroscopy is another excellent technique for the chemical investigations into changes of the catalysts and Nafion™ membrane.[71] Nafion has a distinctive Raman profile in the 0–1000 cm^{-2} Raman shift range therefore any degradation of this material could be potentially monitored by Raman spectroscopy which was previously shown by Krasnova and co-workers for PEM fuel cells.[72]

Physical degradation (*e.g.* diagnoses of microcracks) of the catalyst layers could be conducted by Helium Ion Microscopy (HIM) or Computed Tomography (CT).[73] The information gained from these techniques could also be used to improve catalyst ink formulations. Sub-optimal ink composition could result in a catalyst layer that is not homogeneous, *i.e.* that contains cracks, or is brittle. This would affect the electrolyser measurements; more precisely, the electronic pathway from the catalyst to current collector will be disturbed. The CT studies will allow us to gain further information about the inner layers of the catalyst layer and into the ink formulations/layer deposition and will determine if adjustments need to be made to the ink formulations.

Electrochemical hydrogen pumps hold significant promise for advancing hydrogen compression and separation technologies. Continued progress will depend on the integration of novel materials, the development of standardized testing

procedures, and comprehensive long-term degradation studies. This review provides a practical guide for setting up an experimental EHP system to help address current knowledge gaps. With further research and development, EHPs have the potential to play a crucial role in enabling efficient hydrogen handling across a range of emerging technologies.

Author contributions

Rory Bagacki: writing – original draft, methodology, conceptualization, investigation, data curation. Maximilian Reinhardt: writing – original draft, conceptualization, visualization, software. Rutger Schlatmann: writing – review & editing, supervision. Sonya Calnan: conceptualization, funding acquisition, writing – original draft, writing – review & editing, supervision. Roel Van de Krol: writing – review & editing, supervision. Michelle Browne: conceptualization, funding acquisition, writing – original draft, writing – review & editing, supervision.

Conflicts of interest

There are no conflicts of interest to declare.

Data availability

The data for this highlight are available in the NOMAD database at: **https://nomadhzb-ce.de/nomadoasis/gui/user/uploads/upload/id/6FEEcAURSy2j0crWyi0kxg**.

Acknowledgements

The Helmholtz Association of German Research Centres (HGF) and the Federal Ministry of Education and Research (BMBF), Germany are gratefully acknowledged for supporting the development of solar powered H_2 generation technologies within the frame of the Innovation Pool Project ''Solar H_2: highly pure and compressed'' and the Helmholtz program ''materials and technologies for the energy transition'' (MTET). We gratefully acknowledge the Helmholtz Association's Initiative and Networking Fund (Helmholtz Young Investigator Group VH-NG-1719) for the funding. The authors greatly acknowledge support from the German Federal Ministry of Education and Research in the framework of the project Catlab (03EW0015A/B).

References

1 M. M. Hossain Bhuiyan and Z. Siddique, Hydrogen as an alternative fuel: A comprehensive review of challenges and opportunities in production, storage, and transportation, *Int. J. Hydrog. Energy*, 2025, **102**, 1026–1044, DOI: **10.1016/j.ijhydene.2025.01.033**.
2 J. Brandt, *et al.*, Cost and competitiveness of green hydrogen and the effects of the European Union regulatory framework, *Nat. Energy*, 2024, **9**(6), 703–713, DOI: **10.1038/s41560-024-01511-z**.
3 G. Venugopalan, *et al.*, Electrochemical Pumping for Challenging Hydrogen Separations, *ACS Energy Lett.*, 2022, **7**(4), 1322–1329, DOI: **10.1021/acsenergylett.1c02853**.
4 G. Di Lullo, *et al.*, Large-scale long-distance land-based hydrogen transportation systems: A comparative techno-economic and greenhouse gas emission assessment, *Int. J. Hydrog. Energy*, 2022, **47**(83), 35293–35319, DOI: **10.1016/j.ijhydene.2022.08.131**.
5 M. Niermann, S. Timmerberg, S. Drünert and M. Kaltschmitt, Liquid Organic Hydrogen Carriers and alternatives for international transport of renewable hydrogen, *Renewable Sustainable Energy Rev.*, 2021, **135**, 110171, DOI: **10.1016/j.rser.2020.110171**.
6 C. Jackson, G. Smith and A. R. Kucernak, Deblending and purification of hydrogen from natural gas mixtures using the electrochemical hydrogen pump, *Int. J. Hydrogen Energy*, 2024, **52**, 816–826, DOI: **10.1016/j.ijhydene.2023.05.065**.
7 GASCADE Begins Filling First Section of Repurposed Hydrogen Pipeline Network in Germany'. Accessed: Mar. 25, 2025. [Online]. Available: **https://www.pipeline-journal.net/news/gascade-begins-filling-first-section-repurposed-hydrogen-pipeline-network-germany**.
8 W. Wiebe, T. V. Unwerth and S. Schmitz, Using of an Electrochemical Compressor for Hydrogen Recirculation in Fuel Cell Vehicles, *Fuel Cells*, 2020, **20**(3), 362–369, DOI: **10.1002/fuce.201900090**.
9 K. Fishel, G. Qian, G. Eisman and B. C. Benicewicz, Electrochemical Hydrogen Pumping, in *High Temperature Polymer Electrolyte Membrane Fuel Cells: Approaches, Status, and Perspectives*, ed. Q. Li, D. Aili, H. A. Hjuler and J. O. Jensen, Springer International Publishing, Cham, 2016, pp. 527–540, DOI: **10.1007/978-3-319-17082-4_24**.
10 K. Obata, L. Stegenburga and K. Takanabe, Maximizing Hydrogen Evolution Performance on Pt in Buffered Solutions: Mass Transfer Constrains of H2 and Buffer Ions, *J. Phys. Chem. C*, 2019, **123**(35), 21554–21563, DOI: **10.1021/acs.jpcc.9b05245**.
11 W. Sheng, H. A. Gasteiger and Y. Shao-Horn, Hydrogen Oxidation and Evolution Reaction Kinetics on Platinum: Acid vs Alkaline Electrolytes, *J. Electrochem. Soc.*, 2010, **157**(11), B1529, DOI: **10.1149/1.3483106**.
12 N. A. Godshall, I. D. Raistrick and R. A. Huggins, Relationships among Electrochemical, Thermodynamic, and Oxygen Potential Quantities in Lithium-Transition Metal-Oxygen Molten Salt Cells, *J. Electrochem. Soc.*, 1984, **131**(3), 543–549, DOI: **10.1149/1.2115624**.
13 D. Q. Vu, W. J. Koros and S. J. Miller, Mixed matrix membranes using carbon molecular sieves: I. Preparation and experimental results, *J. Membr. Sci.*, 2003, **211**(2), 311–334, DOI: **10.1016/S0376-7388(02)00429-5**.
14 K. C. Neyerlin, W. Gu, J. Jorne and H. A. Gasteiger, Study of the Exchange Current Density for the Hydrogen Oxidation and Evolution Reactions, *J. Electrochem. Soc.*, 2007, **154**(7), B631, DOI: **10.1149/1.2733987**.
15 D. Schönfuss and L. Müller, On the current-potential curve of a very fast hydrogen evolution process up to high current densities, *Electrochim. Acta*, 1994, **39**(13), 2097–2100, DOI: **10.1016/0013-4686(94)85095-X**.
16 M.-T. Nguyen, S. A. Grigoriev, A. A. Kalinnikov, A. A. Filippov, P. Millet and V. N. Fateev, Characterization of a electrochemical hydrogen pump using electrochemical impedance spectroscopy, *J. Appl. Electrochem.*, 2011, **41**(9), 1033–1042, DOI: **10.1007/s10800-011-0341-9**.
17 M. Nordio, *et al.*, Experimental and modelling study of an electrochemical hydrogen compressor, *Chem. Eng. J.*, 2019, **369**, 432–442, DOI: **10.1016/j.cej.2019.03.106**.
18 C. Casati, P. Longhi, L. Zanderighi and F. Bianchi, 'Some fundamental aspects in electrochemical hydrogen purification/compression', *J. Power Sources*, 2008, **180**(1), 103–113, DOI: **10.1016/j.jpowsour.2008.01.096**.
19 P. J. Sarma, D. Ma, C. L. Gardner and E. Kjeang, Technical evaluation of electrochemical separation of hydrogen from a natural gas/hydrogen mixture, *Int. J. Hydrog. Energy*, 2024, **78**, 610–621, DOI: **10.1016/j.ijhydene.2024.06.262**.
20 G. Sdanghi, J. Dillet, S. Didierjean, V. Fierro and G. Maranzana, Feasibility of Hydrogen Compression in an Electrochemical System: Focus on Water Transport Mechanisms, *Fuel Cells*, 2020, **20**(3), 370–380, DOI: **10.1002/fuce.201900068**.
21 B. L. Kee, *et al.*, Thermodynamic Insights for Electrochemical Hydrogen Compression with Proton-Conducting Membranes, *Membranes*, 2019, **9**(7), 77, DOI: **10.3390/membranes9070077**.
22 J. Zou, *et al.*, Electrochemical Compression Technologies for High-Pressure Hydrogen: Current Status, Challenges and Perspective, *Electrochem. Energy Rev.*, 2020, **3**(4), 690–729, DOI: **10.1007/s41918-020-00077-0**.
23 S. A. Grigoriev, I. G. Shtatniy, P. Millet, V. I. Porembsky and V. N. Fateev, Description and characterization of an electrochemical

hydrogen compressor/concentrator based on solid polymer electrolyte technology, *Int. Workshop Hydrogen Energy*, 2011, **36**(6), 4148–4155, DOI: 10.1016/j.ijhydene.2010.07.012.
24 P. J. Bouwman, *et al.*, (Invited) Electrochemical Hydrogen Compression, *ECS Trans.*, 2014, **64**(3), 1009–1018, DOI: 10.1149/06403.1009ecst.
25 L. Lipp, *Electrochemical Hydrogen Compressor*, United States, 2016, DOI: 10.2172/1235441.
26 'HyET'. [Online]. Available: https://hyethydrogen.com.
27 G. Sdanghi, G. Maranzana, A. Celzard and V. Fierro, Towards Non-Mechanical Hybrid Hydrogen Compression for Decentralized Hydrogen Facilities, *Energies*, 2020, **13**(12), 3145, DOI: 10.3390/en13123145.
28 B. Rohland, K. Eberle, R. Ströbel, J. Scholta and J. Garche, Electrochemical hydrogen compressor, *Electrochim. Acta*, 1998, **43**(24), 3841–3846, DOI: 10.1016/S0013-4686(98)00144-3.
29 R. Ströbel, M. Oszcipok, M. Fasil, B. Rohland, L. Jörissen and J. Garche, The compression of hydrogen in an electrochemical cell based on a PE fuel cell design, *J. Power Sources*, 2002, **105**(2), 208–215, DOI: 10.1016/S0378-7753(01)00941-7.
30 A. Chouhan, B. Bahar and A. K. Prasad, Effect of back-diffusion on the performance of an electrochemical hydrogen compressor, *Int. J. Hydrogen Energy*, 2020, **45**(19), 10991–10999, DOI: 10.1016/j.ijhydene.2020.02.048.
31 G. A. Camara, E. A. Ticianelli, S. Mukerjee, S. J. Lee and J. McBreen, The CO Poisoning Mechanism of the Hydrogen Oxidation Reaction in Proton Exchange Membrane Fuel Cells, *J. Electrochem. Soc.*, 2002, **149**(6), A748, DOI: 10.1149/1.1473775.
32 J. J. Baschuk and X. Li, Carbon monoxide poisoning of proton exchange membrane fuel cells, *Int. J. Energy Res.*, 2001, **25**(8), 695–713, DOI: 10.1002/er.713.
33 G. J. M. Janssen and N. P. Lebedeva, *Carbon dioxide poisoning on proton-exchange-membrane fuel cell anodes*, Netherlands, 2005.
34 J. S. Wainright, J.-T. Wang, D. Weng, R. F. Savinell and M. Litt, Acid-Doped Polybenzimidazoles: A New Polymer Electrolyte, *J. Electrochem. Soc.*, 1995, **142**(7), L121, DOI: 10.1149/1.2044337.
35 Q. Li, R. He, J.-A. Gao, J. O. Jensen and N. J. Bjerrum, The CO poisoning effect in PEMFCs operational at temperatures up to 200 °C, *J. Electrochem. Soc.*, 2003, **150**(12), A1599–A1605, DOI: 10.1149/1.1619984.
36 K. A. Perry, G. A. Eisman and B. C. Benicewicz, Electrochemical hydrogen pumping using a high-temperature polybenzimidazole (PBI) membrane, *J. Power Sources*, 2008, **177**(2), 478–484, DOI: 10.1016/j.jpowsour.2007.11.059.
37 F. Huang, A. T. Pingitore and B. C. Benicewicz, Electrochemical Hydrogen Separation from Reformate Using High-Temperature Polybenzimidazole (PBI) Membranes: The Role of Chemistry, *ACS Sustainable Chem. Eng.*, 2020, **8**(16), 6234–6242, DOI: 10.1021/acssuschemeng.9b07037.
38 F. Liu, *et al.*, Polybenzimidazole/ionic-liquid-functional silica composite membranes with improved proton conductivity for high temperature proton exchange membrane fuel cells, *J. Membr. Sci.*, 2017, **541**, 492–499, DOI: 10.1016/j.memsci.2017.07.026.
39 C. Gao, M. Hu, L. Wang and L. Wang, Synthesis and Properties of Phosphoric-Acid-Doped Polybenzimidazole with Hyperbranched Cross-Linkers Decorated with Imidazolium Groups as High-Temperature Proton Exchange Membranes, *Polymers*, 2020, **12**, 515, DOI: 10.3390/polym12030515.
40 B. J. Kim, S. H. Park, M. L. Díaz-Ramírez and N. C. Jeong, Proton-conducting copper-based MOFs for fuel cells, *Chem. Commun.*, 2025, **61**(18), 3582–3600, DOI: 10.1039/D4CC06378C.
41 S. J. Kim, *et al.*, Characterizations of polybenzimidazole based electrochemical hydrogen pumps with various Pt loadings for H_2/CO_2 gas separation, *Int. J. Hydrog. Energy*, 2013, **38**(34), 14816–14823, DOI: 10.1016/j.ijhydene.2013.08.142.
42 K. Yang, *et al.*, An acid-tolerant metal-organic framework for industrial CO_2 electrolysis using a proton exchange membrane', *Nat. Commun.*, 2024, **15**(1), 7060, DOI: 10.1038/s41467-024-51475-7.
43 J. Ampurdanés, M. Chourashiya and A. Urakawa, Cobalt oxide-based materials as non-PGM catalyst for HER in PEM electrolysis and in situ XAS characterization of its functional state, *Catal. Today*, 2019, **336**, 161–168, DOI: 10.1016/j.cattod.2018.12.033.
44 M. Chhetri, *et al.*, Electrochemical pumps based on ion-pair membranes for separation of hydrogen from low-concentration mixtures, *Nat. Energy*, 2024, **9**(12), 1517–1528, DOI: 10.1038/s41560-024-01669-6.
45 I. Pivac, A. S. Pavasović and F. Barbir, Recent advances and perspectives in diagnostics and degradation of electrochemical hydrogen compressors, *Int. J. Hydrog. Energy*, 2024, **54**, 387–396.
46 T. Molter, *Development of an Electrochemical Separator and Compressor*, United States, 2011, DOI: 10.2172/1012467.
47 L. Schorer, S. Schmitz and A. Weber, Membrane based purification of hydrogen system (MEMPHYS), *Int. J. Hydrogen Energy*, 2019, **44**(25), 12708–12714, DOI: 10.1016/j.ijhydene.2019.01.108.
48 W. Wiebe, T. V. Unwerth and S. Schmitz, Using of an Electrochemical Compressor for Hydrogen Recirculation in Fuel Cell Vehicles, *Fuel Cells*, 2020, **20**(3), 362–369, DOI: 10.1002/fuce.201900090.
49 F. Barbir and H. Görgün, Electrochemical hydrogen pump for recirculation of hydrogen in a fuel cell stack, *J. Appl. Electrochem.*, 2007, **37**(3), 359–365, DOI: 10.1007/s10800-006-9266-0.
50 S. Mrusek, P. Preuster, K. Müller, A. Bösmann and P. Wasserscheid, Pressurized hydrogen from charged liquid organic hydrogen carrier systems by electrochemical hydrogen compression, *Int. J. Hydrogen Energy*, 2021, **46**(29), 15624–15634, DOI: 10.1016/j.ijhydene.2021.02.021.
51 Y. Tao, H. Lee, Y. Hwang, R. Radermacher and C. Wang, Electrochemical compressor driven metal hydride heat pump, *Int. J. Refrig.*, 2015, **60**, 278–288, DOI: 10.1016/j.ijrefrig.2015.08.018.
52 W. Zängler, M. Mohseni, R. Keller and M. Wessling, A tubular electrochemical hydrogen compressor, *Int. J. Hydrogen Energy*, 2024, **66**, 48–54, DOI: 10.1016/j.ijhydene.2024.03.355.
53 Y. M. Hao, H. Nakajima, A. Inada, K. Sasaki and K. Ito, Overpotentials and reaction mechanism in electrochemical hydrogen pumps, *Electrochim. Acta*, 2019, **301**, 274–283, DOI: 10.1016/j.electacta.2019.01.108.
54 B. M. Stühmeier, M. R. Pietsch, J. N. Schwämmlein and H. A. Gasteiger, Pressure and Temperature Dependence of the Hydrogen Oxidation and Evolution Reaction Kinetics on Pt Electrocatalysts via PEMFC-based Hydrogen-Pump Measurements, *J. Electrochem. Soc.*, 2021, **168**(6), 064516, DOI: 10.1149/1945-7111/ac099c.
55 Y. Hao, H. Nakajima, H. Yoshizumi, A. Inada, K. Sasaki and K. Ito, Characterization of an electrochemical hydrogen pump with internal humidifier and dead-end anode channel, *Int. J. Hydrogen Energy*, 2016, **41**(32), 13879–13887, DOI: 10.1016/j.ijhydene.2016.05.160.
56 J. L. Pineda-Delgado, A. U. Chávez-Ramirez, C. K. Gutierrez, S. Rivas, C.-R. Marisela, R. de Jesús Hernández-Cortes, J. A. Menchaca-Rivera and J. F. Pérez-Robles, Effect of relative humidity and temperature on the performance of an electrochemical hydrogen compressor, *Appl. Energy*, 2022, **311**, 118617.
57 J. L. Pineda-Delgado, *et al.*, Energetic evaluations of an electrochemical hydrogen compressor, *J. Energy Storage*, 2022, **55**, 105675, DOI: 10.1016/j.est.2022.105675.
58 L. Vermaak, H. W. J. P. Neomagus and D. G. Bessarabov, Recent Advances in Membrane-Based Electrochemical Hydrogen Separation: A Review, *Membranes*, 2021, **11**(2), 127, DOI: 10.3390/membranes11020127.
59 D. P. Bloomfield and B. S. MacKenzie, *Electrochemical Hydrogen Compressor*, Analytic Power Corp., Santa Fe, NM, 2006.
60 G. Sdanghi, J. Dillet, M. Branco, T. Prouvé and G. Maranzana, An innovative water management system for the electrochemical compression of hydrogen up to 10 MPa, *Int. J. Hydrog. Energy*, 2024, **87**, 117–129, DOI: 10.1016/j.ijhydene.2024.09.019.
61 V. Kumar, P. K. Koorata, U. Shinde, P. Padavu and S. C. George, Review on physical and chemical properties of low and high-temperature polymer electrolyte membrane fuel cell (PEFC) sealants, *Polym. Degrad. Stab.*, 2022, **205**, 110151, DOI: 10.1016/j.polymdegradstab.2022.110151.
62 M. Kostelec, M. Gatalo and N. Hodnik, Fundamental and Practical Aspects of Break-In/Conditioning of Proton Exchange Membrane Fuel Cells, *Chem. Rec.*, 2024, **24**(10), e202400114, DOI: 10.1002/tcr.202400114.
63 Y. Yurko and L. Elbaz, The effect of membrane electrode assembly methods on the performance in fuel cells, *Electrochim. Acta*, 2021, **389**, 138676, DOI: 10.1016/j.electacta.2021.138676.
64 J. Zou, *et al.*, Insights into electrochemical hydrogen compressor operating parameters and membrane electrode assembly degradation mechanisms, *J. Power Sources*, 2021, **484**, 229249, DOI: 10.1016/j.jpowsour.2020.229249.
65 E. Pahon, D. Hissel and N. Yousfi-Steiner, A review of accelerated stress tests dedicated to proton exchange membrane fuel cells – Part I: Fuel cell component level, *J. Power Sources*, 2022, **546**, 231895, DOI: 10.1016/j.jpowsour.2022.231895.

66 I. Bloom, *et al.*, A comparison of Fuel Cell Testing protocols – A case study: Protocols used by the U.S. Department of Energy, European Union, International Electrotechnical Commission/Fuel Cell Testing and Standardization Network, and Fuel Cell Technical Team, *J. Power Sources*, 2013, **243**, 451–457, DOI: **10.1016/j.jpowsour.2013.06.026**.
67 H. A. Gasteiger, J. E. Panels and S. G. Yan, Dependence of PEM fuel cell performance on catalyst loading, *J. Power Sour.*, 2004, **127**(1), 162–171, DOI: **10.1016/j.jpowsour.2003.09.013**.
68 H. Javed, A. Knop-Gericke and R. V. Mom, Structural Model for Transient Pt Oxidation during Fuel Cell Start-up Using Electrochemical X-ray Photoelectron Spectroscopy, *ACS Appl. Mater. Interfaces*, 2022, **14**(31), 36238–36245, DOI: **10.1021/acsami.2c09249**.
69 C. Kaplan, *et al.*, Enhancing CoFe Catalysts with V2CTX MXene-Derived Materials for Anion Exchange Membrane Electrolyzers, *Adv. Funct. Mater.*, 2025, 2503842, DOI: **10.1002/adfm.202503842**.
70 M. P. Browne, C. Domínguez, C. Kaplan, M. E. G. Lyons, E. Fonda and P. E. Colavita, Probing Changes in the Local Structure of Active Bimetallic Mn/Ru Oxides during Oxygen Evolution, *ACS Appl. Energy Mater.*, 2023, **6**(16), 8607–8615, DOI: **10.1021/acsaem.3c01585**.
71 P. C. Okonkwo, I. Ben Belgacem, W. Emori and P. C. Uzoma, Nafion degradation mechanisms in proton exchange membrane fuel cell (PEMFC) system: A review, *Int. J. Hydrogen Energy*, 2021, **46**(55), 27956–27973, DOI: **10.1016/j.ijhydene.2021.06.032**.
72 A. A. Nechitailov, P. Volovitch, N. V. Glebova and A. Krasnova, Features of the Degradation of the Proton-Conducting Polymer Nafion in Highly Porous Electrodes of PEM Fuel Cells, *Membranes*, 2023, **13**, 342, DOI: **10.3390/membranes13030342**.
73 Q. Meyer, *et al.*, Multi-Scale Imaging of Polymer Electrolyte Fuel Cells using X-ray Micro- and Nano-Computed Tomography, Transmission Electron Microscopy and Helium-Ion Microscopy, *Fuel Cells*, 2019, **19**(1), 35–42, DOI: **10.1002/fuce.201800047**.